Int J Appl Earth Obs Geoinformation 77 (2019) 151–161

Contents lists available at ScienceDirect

Int J Appl Earth Obs Geoinformation

journal homepage: www.elsevier.com/locate/jag

Vegetation optical depth at L-band and above ground biomass in the tropical range: Evaluating their relationships at continental and regional scales

Cristina Vittucci[a,*], Gaia Vaglio Laurin[b], Gianluca Tramontana[b], Paolo Ferrazzoli[a], Leila Guerriero[a], Dario Papale[b]

[a] University of Rome Tor Vergata, DICII, Rome, Italy
[b] Tuscia University, DIBAF, Viterbo, Italy

ARTICLE INFO

Keywords:
Forests
SMOS
Biomass
Ecofunctional properties

ABSTRACT

The relationship between vegetation optical depth (VOD) retrieved by L-band SMOS radiometer and forest above ground biomass (AGB) was investigated in tropical areas of Africa and South America. VOD was retrieved from the latest version of level 2 SMOS algorithm, while reference AGB was obtained from a pantropical database, encompassing a large number of ground plot data derived from field surveys conducted on both continents. In Africa and South-America, VOD increased with AGB, reaching saturation at about 350 Mg ha^{-1}. The strength of the relation was improved selecting VOD data in appropriate seasons, characterized by a higher dynamic range of values. The capability of VOD data to estimate AGB was further investigated using Random Forest decision trees, adding to VOD selected climate variables from the Climatic Research Unit (temperature, potential evapotranspiration, and precipitation) and water deficit data, and validating regression tests with ground data from the reference AGB database. The results for the five analyzed years indicate that the best estimates of AGB are obtained by the joined use of VOD and potential evapotranspiration input data, but all climate variables brought an improvement in AGB estimates. AGB estimates were relatively stable for the considered period, with limited variations possibly due to changes in biomass and to data quality of VOD and of climate variables. The VOD signal and estimated AGB were also analyzed according to ecological homogeneous units (ecoregions), evidencing data clusters, partially overlapped to each other, in the VOD - AGB plane.

1. Introduction

Forests worldwide are in a dynamic status, with some regions experiencing accelerated losses and other gains during the last century (Hansen et al., 2013). The monitoring of forest resources and their changes is of paramount importance in a climate change scenario, given forests role as carbon sources or sinks, and considering the relevance of forest ecosystem services (Mori et al., 2017; Ninan and Inoue, 2013). Different forest attributes, such as biomass, biodiversity, leaf traits, and productivity -among others- deserve accurate monitoring, since the larger is the number of the monitored features (with information collected at different spatial and temporal scales), the better is the comprehension of the dynamics of the entire system and its feedbacks to climate-induced changes (Frolking et al., 2009).

Above ground biomass (AGB) is one of the most important parameters, representing the amount of epigean carbon stocked. In the last decade, different studies exploited remote sensing and ground measurements to generate reference data and baseline maps of AGB, or carbon stocks, with continental, pantropical or biome level coverage (e.g. Baccini et al., 2008; Hu et al., 2016; Saatchi et al., 2011; Santoro et al., 2015). These biomass maps, even if referred to years previous to 2010, are valuable tools with considerable spatial resolution (1 square km), usually employed in ecology, forestry, and climate change studies to understand carbon density distribution and validate models (Baccini et al., 2012; Carvalhais et al., 2014; Johnson et al., 2016; Shimel et al., 2015). However, a large uncertainty among the available AGB estimates remains (Mitchard et al., 2013). In the attempt to harmonize the discrepancies, Avitabile et al. (2016) combined two pantropical datasets and used additional field data to produce a new AGB map, having higher accuracy than the original datasets. In the present study this map was selected as reference AGB data.

Despite the use of improved methods, reducing the uncertainty in AGB upscaling remains a challenge; many advantages are expected by the use of remote sensing data, as highlighted by recent initiatives and on-going activities. For example, the GlobBiomass European Space Agency project (www.globbiomass.org; last visited 4 May 2018) is

* Corresponding author.
E-mail address: vittucci@disp.uniroma2.it (C. Vittucci).

https://doi.org/10.1016/j.jag.2019.01.006
Received 26 October 2018; Received in revised form 12 January 2019; Accepted 14 January 2019

producing a global high spatial resolution map for reference year 2010, plus fine scale maps for five countries at 5-year temporal steps. The European Space Agency 'Biomass' Earth Explorer, planned to be launched in 2021, will provide repeated biomass estimates, thus improving our understanding of biomass distribution along time, with almost pantropical coverage.

An important contribution to estimate forest height and AGB can be added by the vegetation optical depth (VOD) data from Soil Moisture and Ocean Salinity satellite (SMOS), the second Earth Explorer Opportunity mission launched in November 2009 by the European Space Agency (ESA) (Kerr et al., 2010; Kerr et al., 2012). SMOS is equipped with an L-band 2-D interferometric radiometer (1400–1427 MHz range); its dual polarization and multi-angular features are used to derive soil moisture (SM) and VOD from brightness temperature measurements. Several studies using L-band radiometers demonstrated that the VOD of forest canopies increases with forest height and/or AGB (Rahmoune et al., 2014; Cui et al., 2015; Vittucci et al., 2016; Konings et al., 2016; Konings et al., 2017; Rodríguez-Fernández et al., 2018). Moreover, Vittucci et al. (2016) reported the linear relationship observed between VOD and forest height to be stable with respect to both temporal and spatial signal variations, with saturation observed only for heights above 30 m. Recently, a INRA-CESBIO VOD product obtained from SMOS L3 data was used to estimate AGB changes in African drylands, as effect of climate impacts (Brandt et al., 2018). Radiometric signatures of previous radiometers, operating at higher frequencies, were used by Liu et al. (2011), who examined two decades of C-band VOD products obtained by the Advanced Microwave Scanning Radiometer (AMSR-E) jointly with Advanced Very High Resolution Radiometer (AVHRR), and concluded that VOD is dependent on woody biomass and can be a useful indicator of deforestation processes. With these AMSR-E C-band data global AGB estimates were also produced, analyzing changes in two decades up to 2013 (Liu et al., 2015). However, recent investigations (Vittucci et al., 2018; Rodríguez-Fernández et al., 2018) found that the trends of C-band VOD saturate at lower values of forest height and/or AGB, with respect to L-band VOD.

AGB is known to vary at regional or biome scale according to abiotic climate variables, which in turn shape the distribution of biotic factors such as soil fertility, species composition and tree allometry (Baker et al., 2004; Chave et al., 2005). Links between biodiversity and biomass were also previously reported (Lasky et al., 2014; Poorter et al., 2015; Strassburg et al., 2010). Several coarse biome classifications exist (e.g. Udvardy, 1975); at finer spatial scale, the ecoregions identified by Olson et al. (2001) incorporate concepts from previous biome classifications, plus information on habitats and species assemblages. These ecological layers can be of help in understanding the response of remote sensing data, such as VOD, or the distribution of estimated AGB in different ecological units.

The present research intends to further clarify the potential of SMOS VOD in providing relevant carbon-related data on Africa and South America homogeneous forests. The aim is not to provide new reference AGB data, but to better analyze SMOS VOD product in these forests, considering that a number of recent studies (Brandt et al., 2018; Rodríguez-Fernández et al., 2018; Vittucci et al., 2018) evidenced a promising L-band VOD role for carbon monitoring. The signal sensitivity to biomass is tested for African and South American tropical forests using 2012 SMOS VOD data and a reference AGB database that encompasses an AGB pantropical map and field plots data (Avitabile et al., 2016). The ability to estimate AGB is evaluated with SMOS VOD data from years included in the 2011–2015 period, also testing the improvement brought to AGB estimates by the addition of climate variables from Climatic Research Unit Time Series (CRU TS) (4.01 release; Harris et al., 2014) and the climate water availability (CWA) from Chave et al. (2014). Averaged SMOS VOD signal and estimated AGB are explored in ecological homogeneous units derived from the ecoregion layers from Olson et al. (2001). To conclude, the possible role of SMOS VOD data to provide relevant biomass and ecological information in forests and/or to complement information provided by other sensors and data networks is reviewed.

2. Materials and methods

2.1. Remote sensing, reference and auxiliary data

The present research was conducted using VOD retrieved from V650 version of level 2 (L2) SMOS data, having an average footprint width -at half maximum of synthetized beam- equal to 43 km (Kerr et al., 2010; Kerr et al., 2012). VOD is a fundamental parameter of the radiative transfer equation adopted in the retrieval algorithm. In that equation it is defined as τ, and the transmissivity of vegetation is given by $\exp(-\tau / \cos\theta)$, where θ is the off-nadir angle of observation. L2 data are provided by ESA in the Icosahedral Equal Area (ISEA) 4H9 equal area grid in swath mode, with inter-node distance equal to 15 km; data are organized in orbits per days, and are quality flagged. Since this research is focused on long term variations, VOD data were monthly averaged at each node to produce time series from 2011 to 2015. Monthly data were further averaged according to years to perform year-based analysis.

Given the size of the VOD pixel grid, that can easily encompass mixed land cover types, a filtering step to retain only homogeneous forested areas was carried out: the Simard et al. (2011) vegetation height map (at 1 km of spatial resolution) was overlapped to VOD grid. We only retained those SMOS grid units for which the average height was higher than 5 m, and this value was exceeded for at least 80% of the grid area. This choice is in accordance with the United Nations Food and Agriculture Organization definition of forests (FAO, 2000): land with tree crown cover (or equivalent stocking level) of more than 10 percent and area of more than 0.5 ha; the trees should be able to reach a minimum height of 5 m at maturity in situ.

The extraction of VOD values at ascending and descending nodes was conducted after the check of different SMOS L2 quality flags, taking into account the probability of Radiofrequency Interference occurrence (RFI-Prob). Nodes having RFI-Prob > 5% were filtered, and the SMOS passes away from the swath center, having less than one hundred of angular samples, were removed.

As reference information, the Avitabile et al. (2016) biomass map was here selected. The map represents the combination of two pre-existing datasets of above ground biomass (Saatchi et al., 2011; Baccini et al., 2012) and is released at 1 km of spatial resolution. It was realized with a data fusion approach, that exploited the pre-existing datasets and an independent field observations dataset, and it was applied in areas (strata) with homogeneous error patterns of the input maps, estimated from the original data and additional covariates. This resulted in estimates of tropical carbon stocks often lower (9–18%) than those presented in the previous datasets. The validation procedure, carried out with 2118 field estimates, showed that the new map has a RMSE of 15–21% that is lower than the input maps and nearly unbiased estimates.

The Climatic Research Unit Time Series (CRU TS) 4.01 release (Harris et al., 2014) has also been used in the present analysis. CRU TS is a freely available 0.5° lat – lon gridded climate dataset, obtained from monthly observations at meteorological stations including all the world's land areas. It covers the period 1901–2016, and is updated every month. Data are merged with meteo station observations collected from several national and international institutions. The CRU TS gridded ground data are derived interpolating site level observations of CRU TS primary variables (precipitation, mean temperature and diurnal temperature range) by a resampling procedure based on the correlation decay distance (CDD), expressed as the distance at which the averaged interstation correlation is no longer significant at the 95% level. The CDD measurement is applied in the interpolation step, to provide the spatial variability of the variable at 0.5° x 0.5° resolution in latitude/

longitude. The evapotranspiration (PET) variable is obtained using a variant of Penman-Monteith method (Harris et al., 2014). This database is widely used in applied climatology and as input to hydrological and biogeochemical models, both at regional and global scales (http://www.cru.uea.ac.uk/about-cru).

The present study uses grids of monthly precipitation, mean near surface temperature (air temperature at 2 m above the soil) and potential evapotranspiration (PET), yearly averaged.

In addition to CRU TS dataset, complementary information on water stress condition was here used: the Climatic Water Availability (CWA) [mm/yr] is the amount of water lost during the dry months (when evapotranspiration exceeds rainfall), provided at 2.5 arc-minute spatial resolution. The CWA is an important predictor of ecosystem response to climatic change (Chave et al., 2014). It is referred to as 'climatic water deficit', as it reflects drought conditions better than annual rainfall, especially in areas where precipitation is concentrated in few months. The CWA is computed over long time periods, referring to forty years of data acquired before 2011, and is considered not to change within the time range of this study. Generally, areas with high water stress have larger negative values, and sites with values close to zero experience no water stress.

All the mentioned reference raster layers, namely the tree height (Simard et al., 2011), the AGB pantropical map (Avitabile et al., 2016), the CRU TS 4.01 release (Harris et al., 2014) and the CWA (Chave et al., 2014) were resampled to match the SMOS grid. Due to the varying spatial resolution of the involved datasets, two different approaches were followed. For data with finer spatial resolution than SMOS VOD (tree height and AGB), values were averaged within the larger SMOS VOD grid. For data with lower resolution with respect to SMOS VOD (climate variables) a nearest neighbor algorithm was used for resampling at SMOS grid scale.

The ecoregions compiled by Olson et al. (2001) were built on the basis of classical biogeography, with inputs from taxonomy, conservation biology, and ecology knowledge. They reflect species and community distribution more accurately than units based on global and regional models derived from gross biophysical features, such as rainfall and temperature, or vegetation structure, or from spectral signatures of remote sensing data. We selected major ecoregions, including a statistically significant number of SMOS data, to explore the trends of VOD and estimated AGB in homogeneous ecological units. For analysis purposes, contiguous ecoregions sharing similar vegetation types in terms of physiognomy, and similar climate patterns in accordance to CRU TS data were aggregated.

2.2. Data analysis and methods

Two preliminary tests were carried out to understand the strength of VOD – AGB relationship along time.

First, the selected Avitabile et al. (2016) AGB map and 2012 average VOD data were used to identify the threshold over which VOD signal showed saturation to increasing forest biomass. The 2012 VOD dataset was selected for this test because it has the shorter time gap with respect to the AGB dataset, but better data quality with respect to previous 2011 year (Oliva et al., 2016). We found an exponential function fitting the VOD vs. AGB relation, and considered the AGB for which VOD reached 90% of its asymptotic value. As a further evaluation, a linear regression function was fit with AGB and VOD as inputs, and the coefficient of determination (R^2) was computed for AGB pixels included in progressively cumulated 25 Mg/ha AGB intervals. In this case, VOD saturation level was selected as the plateau where R^2 reached maximum value, and after which a decrease in the strength of the relationship was observed.

A second test was carried out to identify the season during which the VOD – AGB relationship was stronger in each continent, using a 3-month temporal moving window applied to VOD 2012 dataset. The correlation between 3-month VOD data and AGB map was explored by means of linear regression, selecting the 3-month period having higher R^2 in each continent. In summary, these two preliminary tests allowed to select: i) areas with AGB below the signal saturation limit; ii) months from 2012 year having stronger VOD-AGB relationship, per continent. Then, these two data selection criteria were applied for the estimation of AGB in each continent with SMOS VOD data from different years, from 2011 to 2015, using a Random Forest (RF) statistical data-driven method (Breiman, 2001).

The random Forest (RF) is a supervised "ensemble learning" method, that generates many regression models and aggregates their results. It was developed as an ensemble of decision tree "*the forest*" improved by the introduction of the so called "*bagging*" or "*bootstrap aggregating*". This technique allows to generate several different training subsets, by subsampling uniformly and with replacement the whole set of available data. The outcomes of this procedure, applied to the ensemble of trees, are the improvement of the stability and of the accuracy of the RF method. This ensures the reduction of the output variance and of the overfitting problem with respect to other machine learning approaches (Breiman, 2001). The "*bagging*" method is used to build successive different trees (Breiman, 1996) so that the forest is independently built using the different training subset. The definition process of each training subset by the bootstrap approach leaves some data available to validate the result of a tree. The data not included in each training subset are called Out-Of-Bag (OOB) samples and are in general used to validate the model and to define the associated OOB error, also called Out-Of-Bag estimate. The latter is the mean prediction error on each training sample, computed using only the trees that did not include the same samples in their bootstrap dataset.

During the training phase, each tree is built by a growing process implementing different cascaded nodes, representing the ramification of a tree. The number of trees in the forest is defined before the training by the *n-trees* parameter. At each node, a decision useful to reach the desired solution is evaluated. The decision rules are defined, computing the Gini Index (Breiman, 2001), on the basis of a subset of predictors (i.e. all the inputs variables) randomly chosen at each node. The number of the input variables that are included in the subset of predictors at each node is imposed by the *m-try* parameter. The n-*trees* and the *m-try* are the only two parameters that must be chosen to train a RF model, making its application smoother when compared to more complex machine learning algorithms. After the training phase, the ensemble of the different trees can be applied to predict new outputs simply averaging among the different trees results.

RF was here used to model the relation between the prediction variables (i.e. VOD and the climatological variables) and AGB. For each continent, SMOS nodes were partitioned into training (30%) and validation (70%) sets. The OOB coefficient of determination (OOB R^2) computed on the validation set only was used to evaluate the model results. The tests were repeated after adding CRU 4.0 (precipitation, temperature, evapotranspiration) and CWA data to VOD as input in RF, running separate models for Africa and South America. The *n-tree* and *m-try* values that yielded the lowest RMSE were 1000 and 3 respectively, in both Africa and South America models.

The RF models were initially built considering climatological variables CRU TS of 2012 year only, and the single CWA dataset (not changing in the analyzed period). After this preliminary RF application, the considered inputs were the selected months of SMOS VOD data, and subsequently CRU TS data from 2012 year and the single CWA data were added. The RF models were always trained using 2012 input data, and then applied to datasets from the other years.

The ground records from field surveys used by Avitabile et al. (2016) for independent validation of their AGB estimate were also used here to further validate the RF AGB estimates of a selected year (2014). Specifically, the South America and Africa ground data were separately averaged according to SMOS grid, retaining only those nodes associated to a minimum of 3 field records.

Finally, SMOS VOD 2014 values were explored in the selected

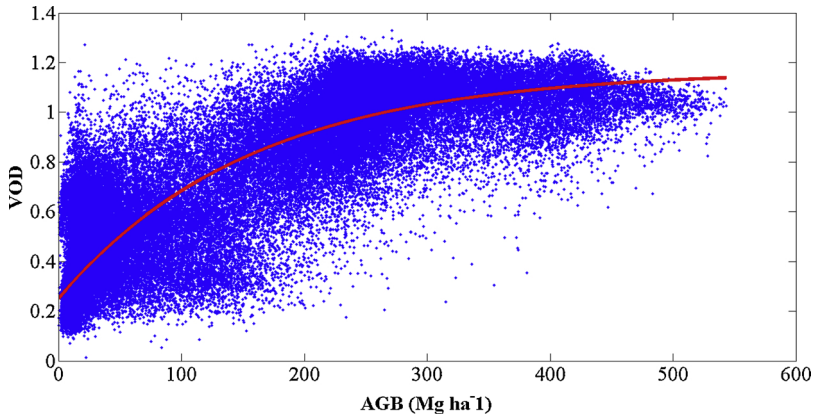

Fig. 1. VOD vs AGB scatterplot and exponential fitting. VOD data are from 2012 year, from Africa and South America forests.

homogeneous ecological units. The total estimated AGB (in Pg) for that year was also computed for the selected ecoregions.

3. Results

After excluding VOD data from non-forests (vegetated areas below the 5 m trees height threshold), the obtained study area resulted to have an extension equal to 43.4% (Africa) and 70.9% (South America) of the continental area considered by the Avitabile et al. (2016) reference AGB map.

The exponential fitting of VOD vs AGB for both Africa and South America continents was obtained using the function (with AGB unit in Mg ha^{-1}):

$$VOD = 0.25 + 0.92\ [1\text{-}\exp(-0.0064\ AGB)] \quad (1)$$

characterized by a determination coefficient (R^2) equal to 0.71 and a RMSE equal to 0.165 VOD units, respectively. The VOD vs. AGB scatterplot and the associated exponential fitting function is presented in Fig. 1; VOD reaches 90% of its asymptotic value at AGB = 360 Mg ha^{-1}. As a linear regression function indicates that the maximum coefficient of determination is obtained at AGB equal to 350 Mg ha^{-1} (R^2 = 0.72), this was considered as the saturation limit for the present study. These tests were carried out using the 2012 VOD dataset, being the second year for which SMOS data are fully available but with less interference problems than in 2011. The test was repeated with other years too, obtaining minimal differences in R^2 (at second decimal place, unreported tests), and confirming a stable signal response.

When the 3-month temporal moving window was applied to the continental datasets separately, filtered to retain only areas with AGB < 350 Mg ha^{-1}, differences in the strength of the VOD-AGB relationship along seasons emerged. For Africa, the 3-month period having higher coefficient of determination (R^2 = 0.65, 33813 samples) was Mar.-May, while for South America it resulted to be Oct.-Dec. (R^2 = 0.69; 45291 samples). These periods in general correspond to months in which –at continental level- VOD values are lower in dry forests and woodlands ranges, with consequent increase of dynamic range. Fig. 2 shows the seasonal variability in the VOD-AGB relationships: it resulted minimal in both continents, as recorded R^2 changes were in the order of 0.05 in Africa and 0.07 in South America. The analysis included a number of samples equal to about 55,000 for Africa and 66,000 for South America, with seasonal variations lower than 0.1% in both cases.

Random Forest (RF) algorithm was initially used to evaluate how much of the variability in AGB data (with 350 Mg ha^{-1} threshold) is explained by the CRU TS and CWA variables, using single variables as input in the models, without using SMOS VOD (Table 1). AGB models were trained with one climate variable at a time from 2012 year, except for CWA that does not vary in the analyzed period. Then these models

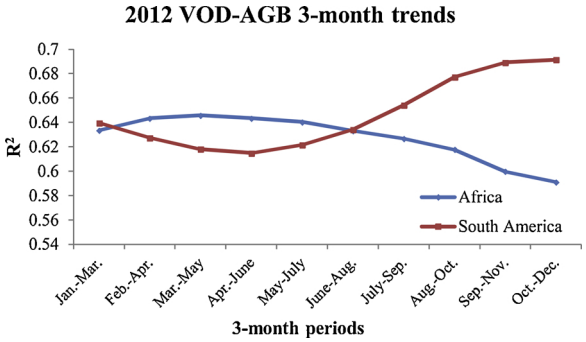

Fig. 2. Seasonal variability in 2012 VOD-AGB (up to 350 Mg ha^{-1}) relationship for Africa and South America.

were run using CRU TS and CWA variables from different years, and validated with Avitabile AGB dataset, partitioned in 30% for model training and 70% for model validation. The corresponding OOB R^2 values for each year are reported in separate rows of Table 1. Since CWA refers to forty years of data acquired before 2011, only one OOB R^2 is reported for this variable.

These results show that climate variables partly contribute to shape regional variations in AGB, with PET and precipitation providing better results for both continents. These reported relationships are moderate, and characterized by very high RMSE values. The correlation coefficients among CRU variables were also computed: for both continents, values resulted < 0.4 between precipitation and PET, and up to 0.55 for correlations with the temperature variable.

The results of further Random Forests models, performed to test how well SMOS VOD explains the variability in AGB data (under the 350 Mg ha^{-1} threshold), with and without the addition of yearly averaged CRU TS 4.01 and CWA data to VOD from selected months, are illustrated in Table 2. Also in this case the RF models were trained with 2012 data (except for CWA single dataset) and 30% Avitabile et al. (2016) training set, run using input datasets from the different years, and validated using the 70% Avitabile et al. (2016) validation set. Differences in OOB R^2 among years resulted minimal, with lower values found in 2011 and 2015. The addition of CRU TS data improved the model accuracies more than CWA; the highest OOB R^2 values are obtained adding potential evapotranspiration (PET) to VOD in Africa (OOB R^2 = 0.79) and precipitation in South America (OOB R^2 = 0.8); the lowest RMSE is always obtained when using PET CRU variable (third column in Table 2).

Fig. 3 shows a comparison of the retrieved 2014 AGB based on VOD and PET data, and Avitabile et al. (2016) maps (up to 350 AGB Mg ha^{-1}) for the two continents. Areas of high, intermediate and low biomass coarsely coincide. When looking at fine ranges of AGB values,

Table 1
Random Forest OOB R^2 values for AGB models using CRU TS and CWA variables as input. In parenthesis, the RMSE values in Mg ha $^{-1}$ are also provided.

	R^2 Temperature	R^2 PET	R^2 Precipitation	R^2 CWA
Africa				*0.47 (77.44)*
Africa 2011	*0.41 (80.47)*	*0.52 (72.17)*	*0.50 (72.93)*	
Africa 2012	*0.41 (79.07)*	*0.52 (72.30)*	*0.53 (70.61)*	
Africa 2013	*0.41 (79.32)*	*0.52 (70.67)*	*0.51 (71.84)*	
Africa 2014	*0.41(78.61)*	*0.55 (69.84)*	*0.56 (68.91)*	
Africa 2015	*0.40 (80.01)*	*0.55 (68.87)*	*0.46 (75.16)*	
S. America				*0.46 (77.62)*
S. America 2011	*0.39 (68.31)*	*0.46 (64.99)*	*0.55 (58.87)*	
S. America 2012	*0.39 (68.30)*	*0.49 (62.10)*	*0.58 (56.65)*	
S. America 2013	*0.42 (67.22)*	*0.48 (63.76)*	*0.61 (55.25)*	
S. America 2014	*0.39 (69.49)*	*0.47 (64.00)*	*0.55 (59.56)*	
S. America 2015	*0.43 (66.75)*	*0.45 (65.24)*	*0.52 (60.69)*	

it can be noted that in the retrieved AGB map few areas reach the maximum AGB values with respect to the reference map, implying a possible underestimation of the VOD plus PET model.

An additional validation of AGB estimated by means of VOD plus PET 2014 data was performed using AGB independent data from field measurements, as provided by Avitabile et al. (2016). The validation result indicates good agreement (R^2 = 0.63, Fig. 4) between estimated and field AGB records, but suggests the possible AGB underestimation observed in previous Fig. 3.

The total amount of forest biomass (Pg) was estimated in the two continents from 2011 to 2015 using selected SMOS VOD 3-month periods and yearly averaged PET data for each year; PET was selected as its use leads to lower RMSE then the other climate variables, at comparable R^2 values (as reported in Table 2). A total of 55014 SMOS VOD samples were used for Africa and 66451 for South America, representing 43.4% and 70.9% of the area considered in the AGB reference map, respectively.

The differences in total AGB among years resulted limited. Considering the uncertainty associated to the estimates, and the fact that RF models for different years are trained and validated with the same AGB reference data, and referred to a period before 2010, these differences are too low to draw conclusions about temporal trends of continental AGB. In fact, different factors can contribute to the observed AGB yearly variations, including SMOS VOD and PET data quality.

The Olson et al. (2001) ecoregions were selected and aggregated to compose 8 units for Africa and 17 for South America. Mean 2014 VOD values, VOD coefficients of variation (which is an indicator of the VOD homogeneity within the ecoregion) and numbers of samples per ecoregion guided the aggregation of the units. The larger number of units identified in South America with respect to Africa reflects the higher number of ecoregions delineated by the Olson et al. (2001) approach, as well as the environmental heterogeneity of this continent. VOD values from other years (from 2011 to 2015) were similar to those reported for 2014, with no significant difference among years for any of the tested unit (not reported tests). The following Fig. 5 illustrates the African units that were considered for the analysis.

According to Table 4, Lowland and Swamp forests, which are the rainforests included in the tropical wetter range, show the highest VOD values. As expected, the forest-savanna unit surrounding the Congo basin, characterized by lower rainfall and less dense and tall forests, display a lower VOD value, which further decreases by similar amount in the dry forests of the Miombo woodlands located south of the equator, and in the dry and fragmented forests of Guinean Forest-Savanna mosaics of Western Africa. The lowest VOD values are found in the two Savannas and Bushlands/Thickets units.

Based on VOD signal similarity, the units were further aggregated in the four units considered in Fig. 6, which shows the scatterplot between SMOS VOD 2014 values and AGB from the reference map.

The scatterplot in Fig. 6 displays clear data clusters, with limited overlap between Miombo Woodland + Guinean Forest Savannah and the Lowland and Swamp forests. These two latter units, having higher AGB values, are well discriminated according to VOD values. Conversely, other ecoregions characterized by lower AGB show overlap in VOD values, which in most cases are below 0.6 and characterized by large variance, especially in the case of the Forest Savanna Mosaic unit.

According to the results in Fig. 7, the rainforest unit hosts the larger part of continental AGB, more than two times the AGB of the other summed units. The Forest Savanna Mosaic unit, surrounding the Congo basin, also includes considerable forest AGB stocks, even if it only represents about ¼ of that of the rainforest area. The biomass included in Miombo woodlands plus Guinean forest-savannas is lower but not so different in amount from that included in the forests of Forest Savanna Mosaics; conversely, much lower AGB is stored in the forests of the Savannas and Bushland units.

Fig. 8 illustrates the 17 South America ecoregions or aggregated units. Mean VOD 2014 values, coefficient of variation, and samples number for these units are shown in Table 5.

In South America, higher VOD values are found in northern, western, southwestern and Guianan piedmont Moist forests. Still very high

Table 2
Random Forest OOB R^2 values (areas up to 350 AGB Mg ha^{-1}), obtained using as input VOD averaged in March-May period for Africa, and August-October for South America, plus CRU TS and CWA yearly averaged data. In parenthesis, RMSE values in Mg ha $^{-1}$.

	R^2 VOD	R^2 VOD + Temperature	R^2 VOD + PET	R^2 VOD + Precip.	R^2 VOD + CWA
Africa 2011	0.69 *(57.51)*	0.78 *(50.50)*	0.77 *(49.59)*	0.75 *(51.35)*	0.70 *(56.80)*
Africa 2012	0.69 *(57.46)*	0.76 *(50.71)*	0.77 *(49.54)*	0.76 *(51.76)*	0.71 *(57.33)*
Africa 2013	0.69 *(57.15)*	0.77 *(50.11)*	0.76 *(48.62)*	0.76 *(50.83)*	0.72 *(57.38)*
Africa 2014	0.72 *(55.01)*	0.77 *(49.21)*	0.79 *(48.41)*	0.78 *(49.16)*	0.71 *(56.96)*
Africa 2015	0.68 *(58.18)*	0.75 *(51.87)*	0.77 *(49.21)*	0.74 *(52.57)*	0.70 *(57.10)*
S. America 2011	0.57 *(57.50)*	0.65 *(61.62)*	0.72 *(56.92)*	0.70 *(59.64)*	0.71 *(56.94)*
S. America 2012	0.71 *(47.90)*	0.77 *(42.17)*	0.79 *(40.23)*	0.80 *(40.41)*	0.72 *(56.68)*
S. America 2013	0.70 *(47.79)*	0.76 *(42.54)*	0.79 *(39.33)*	0.80 *(40.22)*	0.72 *(55.16)*
S. America 2014	0.69 *(49.97)*	0.77 *(43.03)*	0.79 *(41.20)*	0.78 *(41.54)*	0.71 *(56.20)*
S. America 2015	0.58 *(49.37)*	0.68 *(60.86)*	0.73 *(55.32)*	0.70 *(58.98)*	0.71 *(56.74)*

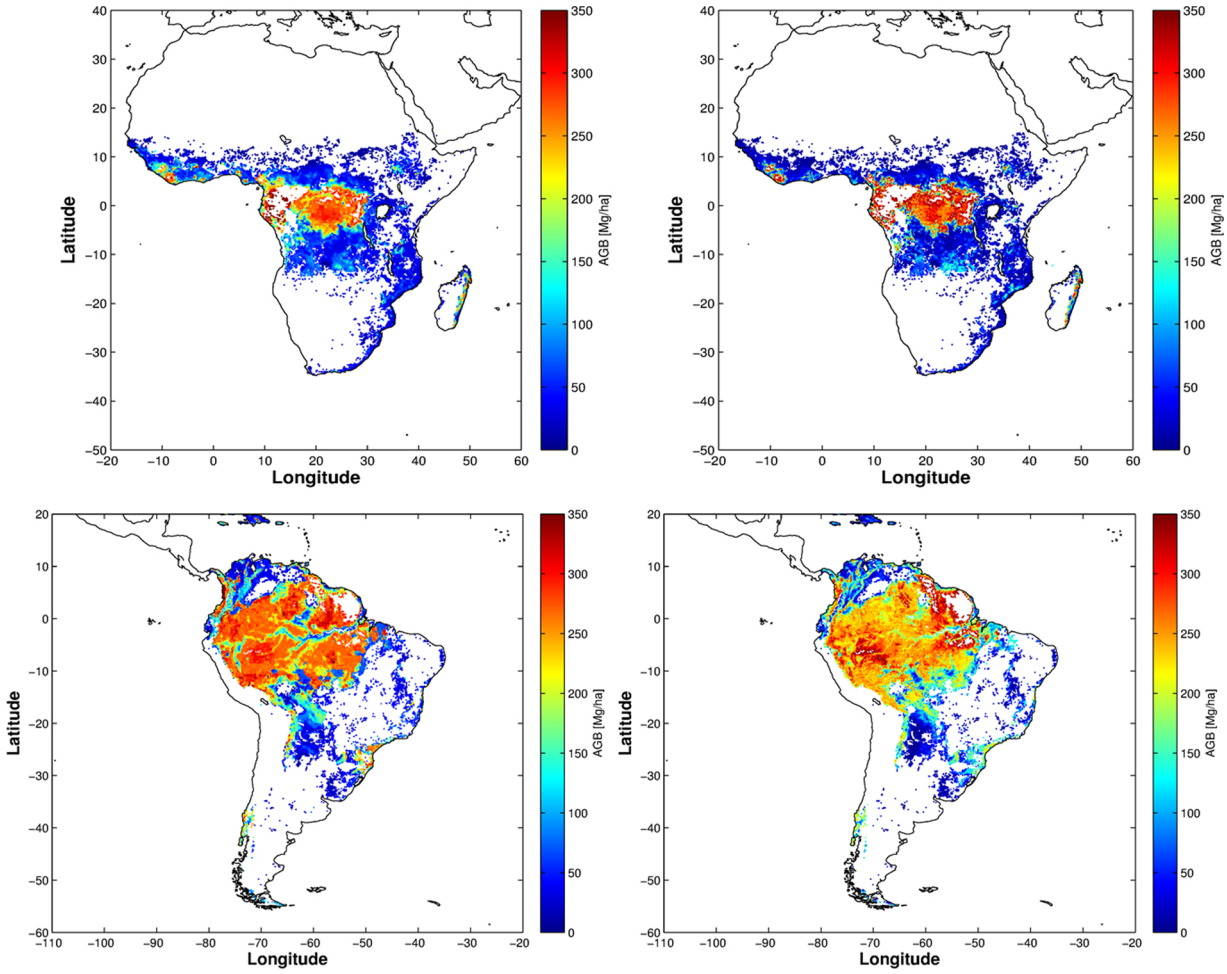

Fig. 3. Upper left: Africa AGB map retrieved using March-May VOD and CRU PET 2014 data. Upper right: Avitabile et al. (2016) AGB map for Africa. Lower left: South America AGB map retrieved using October-December VOD and CRU PET 2014 data. Lower right: Avitabile et al. (2016) AGB map for South America.

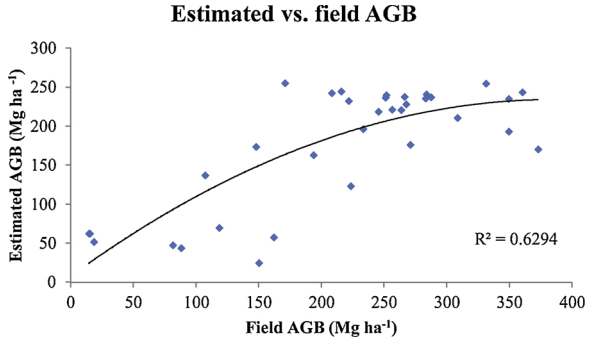

Fig. 4. Scatterplot between AGB values retrieved using VOD plus CRU PET 2014 data and field AGB values as provided by Avitabile et al. (2016) for Africa and South America. Field values were averaged according to SMOS grid, and a logarithmic curve was used as best fit.

VOD values occur in eastern, southeastern Moist and Swamp forests. The mentioned units host the densest and wettest forests of this continent, surrounding the Amazonian basin. A lower VOD value occurs in the Mato Grosso seasonal forests, having dry forest features. Then, intermediate VOD values are found in the Araucaria moist forests, dominated by conifers, and Dry Chaco forests, located in semi-arid plains. Slightly lower VOD values are found in: forests of the wet Chaco, characterized by patches of dry forests alternated with palm savannahs and wetlands; forest of the dry Cerrado unit; and those of the Alto Paranà unit, in which mainly secondary dry and semi-deciduous forests are present. A further decrease in VOD is observed for forests occurring in the Atlantic dry region, and in Caatinga and Llanos units. The lowest values are found in the forests of the Uruguayan savanna ecoregion.

Some of the South America Olson et al. (2001) ecoregions included a limited number of VOD samples, thus of continuous forest above 5 m height. A threshold of 670 samples (corresponding to the smallest of the African units) was arbitrarily set, to exclude smaller units prior to the further aggregation performed in accordance with similarity in mean VOD 2014 value and the coefficients of variation. The aggregation process resulted in 5 units, used to produce the scatterplot (Fig. 8) between SMOS 2014 VOD and data from the reference AGB map (Fig. 9).

In South America, the Northern moist + Southwestern moist + Western moist + Guianan piedmont forests show higher values of both AGB and VOD, composing a well-defined cluster. For other Moist (East and Southeastern moist) and Swamp forests, as well as for Mato Grosso, VOD values resulted highly variable: two different clusters (low and high AGB) emerged, a fact that deserves further investigation. The lower AGB are observed in Chaco, with high VOD values variance, and in the Cerrado unit, with saturation of the VOD signal. Fig. 10 shows the total amount of AGB in the five different South America units. The AGB stored in the rainforest area of the Amazonian basin represents by far the majority of the biomass of this continent.

4. Discussions

The initial results here obtained indicate that VOD saturation to

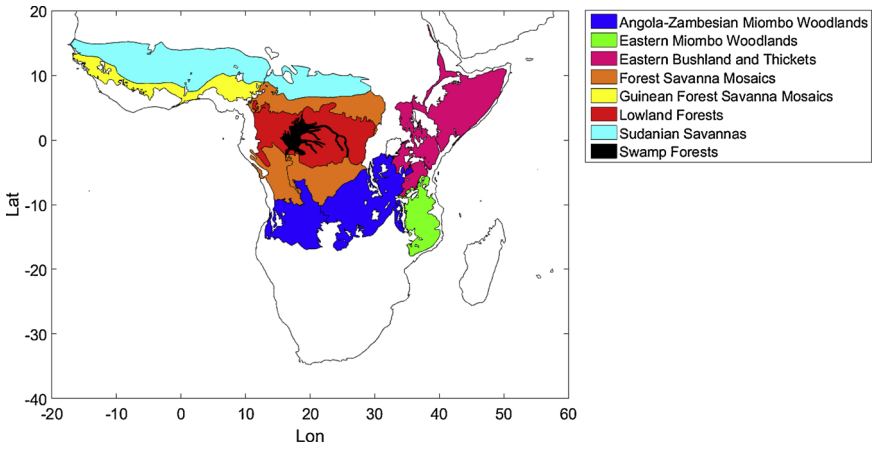

Fig. 5. African ecoregions or aggregated units from Olson et al. (2001).

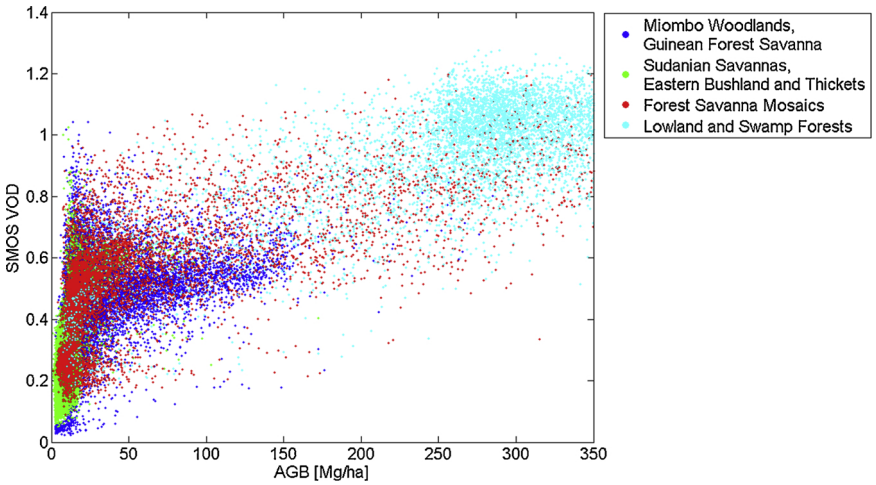

Fig. 6. Scatterplot between averaged 2014 VOD values and AGB, for four aggregated units based on Olsen et al. (2001) ecoregions.

AGB occurs at about 350 Mg ha^{-1}, a value close to what was found by Rodríguez-Fernández et al. (2018) using VOD from the SMOS-IC product. The 350 Mg ha^{-1} saturation limit is considerably high, and is the upper bound used in most AGB reference datasets (Baccini et al., 2008; Saatchi et al., 2011). Conversely, lower saturation limits are obtained when using Synthetic Aperture Radar (SAR) backscattering data. The highest values are achieved at P band, but do not exceed 200 Mg ha-1 (Imhoff, 1995; Santos et al., 2003; Wang et al., 2006).

Previous attempts to relate VOD data to AGB found varied levels of signal saturation. Rahmoune et al. (2014) study, based on SMOS 2011 data with a reference biomass map from United States, found a positive

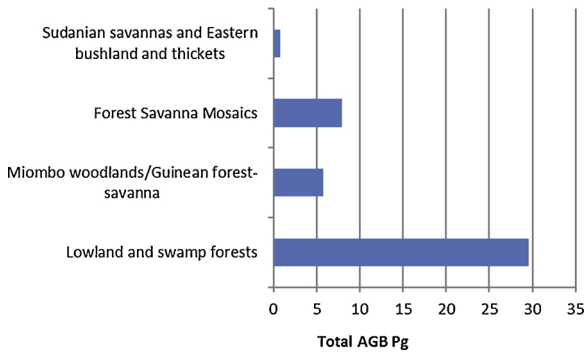

Fig. 7. Total AGB estimated in Africa for the 2014 year, in four aggregated units from Olson et al. (2001) ecoregions.

increasing trend of optical depth vs biomass, but for a limited low range of AGB values. Vittucci et al. (2016) found moderate relationship between VOD data and Avitabile et al. (2016) biomass map (R^2 = 0.60 for Africa and 0.63 for South America). However, both previously mentioned papers were based on a preliminary version of the SMOS algorithm (v 620), and used limited time slots (4 or 8 days). Brandt et al. (2018) used the INRA (Institut National de la Recherche Agronomique) - CESBIO (Centre d'Etudes Spatiales de la BIOsphère) (IC) L-VOD dataset, which is a modification of the SMOS L3 algorithm, to evaluate carbon density changes in Africa from 2010-2016: they did not report any saturation effect using Baccini et al. (2008) reference data. For Africa biomass estimation, Rodríguez-Fernández et al. (2018) also used the SMOS VOD IC dataset, and reported high linear correlation and absence of saturation when using as reference Baccini et al. (2008) and Saatchi et al. (2011) maps. The same authors obtained a non-linear relationship and dispersion at high carbon density (> 300 Mg/ha) when using as reference the Avitabile et al. (2016) and the Bouvet et al. (2018) savannas and woodlands datasets.

Within the saturation level found in the present research, most of the forested areas in the tropical range are included. This positive result is in part due to the use of dense temporal series that are known to increase the sensitivity of L-band data to AGB (Englhart et al., 2011; Vittucci et al., 2016). However data from lower frequency bands might still be needed to characterize areas with extremely high biomass values, such as some of the tropical wetter areas also included in the Avitabile et al. (2016) dataset.

Africa and South America forests belong to areas characterized by

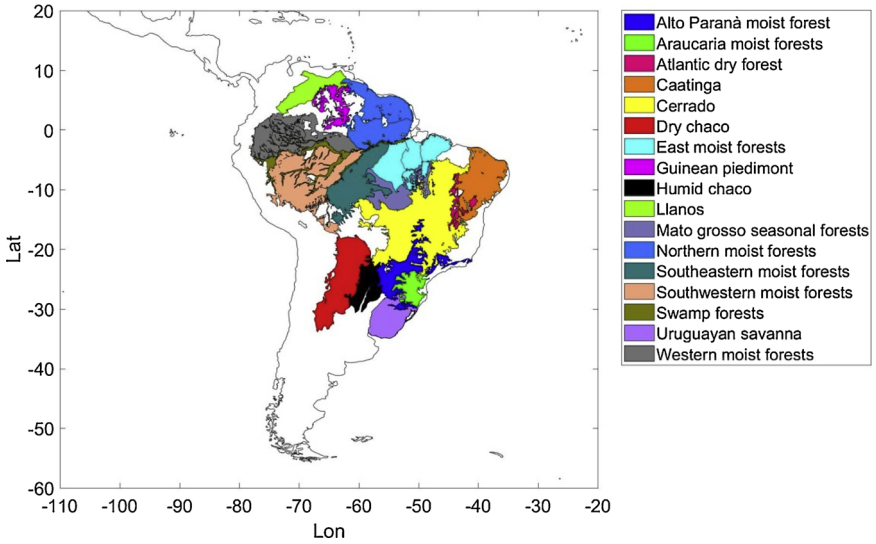

Fig. 8. South American aggregated units from Olson et al. (2001) ecoregions.

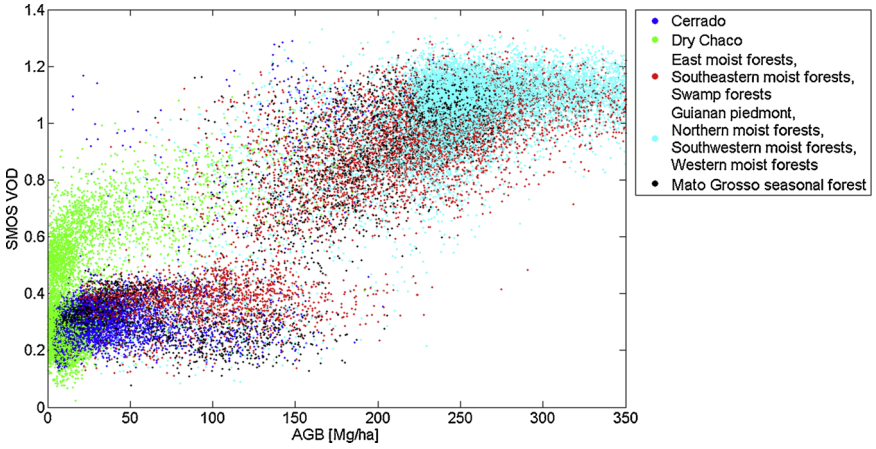

Fig. 9. Average 2014 VOD vs. AGB Scatterplot, with identification of aggregated South American ecoregions.

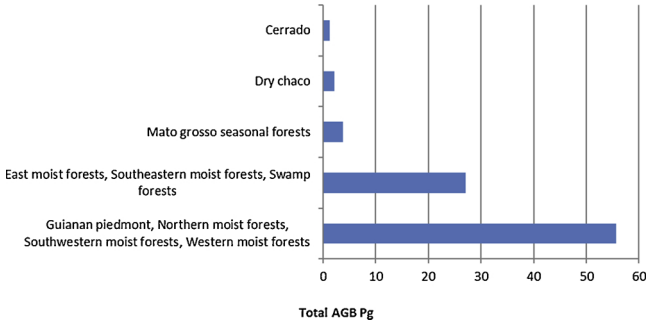

Fig. 10. Total AGB estimated for the 2014 year in 5 South America ecoregions or aggregated units.

Table 3
Total AGB estimated in Africa and South America forests selecting SMOS nodes with forest height > 5 m, with coverage > 80% of the node. AGB was estimated using VOD and CRU PET input data.

Year	Africa forests total AGB (Pg)	South America forests total AGB (Pg)
2011	62.65	149.44
2012	65.50	150.50
2013	63.93	149.85
2014	63.84	150.95
2015	62.34	148.40

different climate seasonality regimes (Munzimi et al., 2015; Nicholson, 2000), with non-seasonal as well as single, dual-, and multiple wet season patterns (Herrmann and Mohr, 2011; Moron et al., 1995; Reboita et al., 2010). Total or seasonal rainfall amount is known to exert a strong control on vegetation structure (Good and Caylor, 2011), biomass density (Álvarez-Dávila et al., 2017; Stegen et al., 2011; Wagner et al., 2012), with also ecosystem carbon fluxes responding to changes in rain pulses (Williams et al., 2009). The rainfall regimes influence canopy water content, which in turn can have an effect on L-band signal response and contributes to shape the overall VOD-AGB relationship. Here, only minimal seasonal variations in the strength of the correlation between VOD and AGB were observed at continental level, but the possible occurrence of different trends at a finer spatial scale of analysis deserves further investigation. Recently, a 4-year analysis characterizing VOD trends in selected regions was conducted by Vittucci et al. (2018). These authors found: a high VOD value along all the year in rainforests of Peru; a lower VOD value in dry woodlands of Argentinian Chaco during months of scarce precipitations; and a delay between precipitation and VOD maximum value in dry forests of Zambia and Angola. The months of best VOD-AGB correlation here selected, for Africa March to May and for South America October to December, in general correspond to months in which –at continental level- VOD values are usually lower in dry forests and woodlands

Table 4
VOD average value, coefficient of variation, and number of samples for 8 African ecoregions or aggregated units from Olsen et al. (2001).

Africa Aggregated Unit	Original Ecoregions	Average VOD 2014	Coefficient of variation	VOD samples number
Lowland Forests	Northwestern + Northeastern + Central + Southern Congolian Lowland Forests	0.99	0.15	6930
Swamp Forest	Western + Eastern Congolian Swamp Forests	0.96	0.16	1011
Forest Savanna Mosaic	Northern + Southern + Western Congolian Forest-Savanna Mosaics	0.59	0.32	6157
Guinean Forest Savanna Mosaics	Guinean Forest Savanna Mosaics	0.49	0.37	1318
Angola-Zambesian Miombo Woodlands	Angolan + Central Zambiesian Miombo Woodlands	0.48	0.27	6248
Eastern Miombo Woodlands	Eastern Zambiesian Miombo Woodlands	0.47	0.30	1724
Sudanian Savannas	East + West Sudanian Savannas	0.38	0.45	1913
Eastern Bushland and Thickets	Northern + Somali + Southern Acacia-Commiphora Bushlands and Thickets	0.31	0.26	672

Table 5
VOD 2014 average value, coefficient of variation, and number of samples for South America ecoregions or aggregated units from Olsen et al. (2001).

South America Aggregated Unit	Original ecoregions	Average VOD 2014	Coefficient of variation	VOD samples number
Northen moist forests	Uatuma-Trombetas + Guianan moist forests	1.07	0.14	4666
Southwestern moist forests	Juruá-Purus + Purus-Madeira + Southwest Amazon moist forests	1.05	0.12	5585
Western moist forests	Caqueta + Napo + Japurá-Solimoes-Negro + Solimões-Japurá moist forests	1.04	0.13	4371
Guianan piedmont	Guianan piedmont and lowland moist forests	1.03	0.17	1100
Swamp forest	Iquitos + Purus + Gurupa + Monte Alegre varzeás	0.96	0.15	1608
East moist forests	Xingu-Tocantins-Araguaia + Tocantins/Pindare + Tapajós-Xingu moist forests	0.91	0.30	3513
Southeastern moist forests	Madeira-Tapajós moist forests	0.88	0.30	3558
Mato grosso seasonal forests	Mato grosso seasonal forests	0.76	0.41	1401
Araucaria moist forests	Araucaria moist forest	0.66	0.38	380
Dry chaco	Dry chaco	0.62	0.24	1820
Humid chaco	Humid chaco	0.54	0.39	265
Alto Paranà moist forest	Alto Paranà moist forest	0.51	0.53	417
Cerrado	Cerrado	0.48	0.63	920
Atlantic dry forests	Atlantic dry forests	0.37	0.51	161
Caatinga	Caatinga	0.34	0.32	263
Llanos	Llanos	0.32	0.44	427
Uruguayan savanna	Uruguayan savanna	0.22	0.32	461

ranges. In these months, a higher dynamic range of VOD is observed, with lower values in drier forests that causes an increase in the correlation of VOD with AGB. This difference in seasonal VOD sensitivity to biomass, observed at smaller scales, might be a chance to improve the accuracy of regional AGB estimates, by means of the selection of specific time series and monthly data.

An improvement in the accuracy of the biomass estimates was obtained adding to VOD any of the CRU TS variables. The use of PET was preferred as it produced lower RMSE, with the VOD plus PET model explaining almost 80% of the variation in African and South American forest biomass. PET variable represents the local environmental evapotranspiration requirements imposed by climate conditions (radiation, temperature, wind, relative humidity): this variable summarizes overall climate information, thus the limits imposed by local climate to vegetation development. Instead, the use of CWA dataset brought limited improvement in accuracy of AGB estimates: the extent of forests not affected by high water stress is large in the tropics, and possibly this layer can help more when estimating biomass in dry regions.

The aim of this research is not to provide new reference biomass values, also considering the uncertainty propagated from the reference map to the final estimates, but to help in clarifying pros and cons in SMOS VOD data use for large scale and repeated biomass monitoring. The area here sampled represents only a portion (43.4% for Africa and 70.9% for South America, respectively) of the study area of Avitabile et al. (2016), since it refers solely to full forest structures, characterized by a height above 5 m by definition and having large and continuous spatial extent such as to cover a minimum of 80% of a SMOS node. These features should be taken into account when comparing the retrieved AGB with the reference dataset. Here the total biomass (Table 3) resulted equal to 76% and 93% of the total AGB reported by Avitabile et al. (2016) for Africa and South America, respectively. The larger discrepancy found in Africa might be due to a larger amount of biomass stored in lower vegetation formation (below 5 m height) and in non-continuous or fragmented forests in Africa with respect to South America.

The analysis of 2014 VOD yearly values in selected ecoregions or aggregated units from Olson et al. (2001) showed that in general VOD decreases from wetter to drier regions. Some units showed unique values, but other had similar optical depth ranges. The coefficients of variation indicate a more stable signal in wetter forest ranges in both continents, such as moist, lowland and swamp forests, and higher signal dynamic in drier ranges. In South America, the higher VOD values observed in piedmont, western and northern Amazonia ranges (mean optical depth from 1.03 to 1.07) seem to partially agree with the regional AGB variations mapped by Saatchi et al. (2009), who reported the western, northern, and Andean foothills as the most productive forests in South America.

The VOD vs. AGB scatterplots for ecoregions or units derived by Olson et al. (2001) display some clear data clusters for those units encompassing large amounts of biomass in both continents. Instead, for some ecoregions, such as African Savannas, African Eastern bushland and Thickets, and South American Chaco, there is an appreciable range of VOD values, although the AGB estimated by Avitabile et al (2016) is uniformly low. This result deserves further investigation, but there are preliminary indication that for the clusters clearly evidenced SMOS can be a useful tool to monitor biomass at regional level. Further improvement could be derived by selecting the SMOS VOD best time series according to considered ecological units.

5. Conclusions

Overall, the results here presented proved that L-band VOD can be usefully employed to estimate tropical forest biomass distribution at continental scale, advancing the previous efforts that established a correlation between VOD signal dynamics and AGB. The availability of VOD dense time series allowed the selection of data from specific months, also according with rainfall patterns that are known to influence both biomass distribution and signal response. This approach is promising, as it can improve the VOD-AGB relationship especially when performing analysis for specific regions. The addition of climate information was useful in improving the accuracy of the AGB estimates in Africa and South America. A relevant variability in the distribution of carbon stocks of tropical forests is already recognized, and calls for regional scale monitoring of biomass. The preliminary tests conducted with ecoregions or aggregated units from Olson et al. (2001) suggest that VOD can produce valuable information also at this scale. Overall, additional efforts in calibration and validation of these initial findings at finer ecoregional scale are necessary, but the results are promising and indicate that SMOS can be a valuable tool to support the monitoring of tropical homogeneous forests from global to regional scale.

Acknowledgments

Work partially supported by ESA, European Space Agency, under Contract No. 4000113119/15/I-SB0. G.V.L and D.P. acknowledge the European Union for supporting the BACI project funded by the EU's Horizon 2020 Research and Innovation Programme under grant agreement #640176

References

Álvarez-Dávila, E., Cayuela, L., González-Caro, S., Aldana, A.M., Stevenson, P.R., Phillips, O., et al., 2017. Forest biomass density across large climate gradients in northern South America is related to water availability but not with temperature. PLoS One 12 (3) e0171072.

Avitabile, V., Herold, M., Heuvelink, G., Lewis, S.L., Phillips, O.L., Asner, G.P., et al., 2016. An integrated pan-tropical biomass map using multiple reference datasets. Glob. Chang. Biol. 22 (4), 1406–1420.

Baccini, A., Laporte, N., Goetz, S.J., Sun, M., Dong, H., 2008. A first map of tropical Africa's above-ground biomass derived from satellite imagery. Environ. Res. Lett. 3.

Baccini, A.G.S.J., Goetz, S.J., Walker, W.S., Laporte, N.T., Sun, M., Sulla-Menashe, D., et al., 2012. Estimated carbon dioxide emissions from tropical deforestation improved by carbon-density maps. Nat. Clim. Change 2 (3), 182.

Baker, T.R., Phillips, O.L., Malhi, Y., Almeida, S., Arroyo, L., Di Fiore, A., et al., 2004. Variation in wood density determines spatial patterns in Amazonian forest biomass. Glob. Chang. Biol. 10 (5), 545–562.

Bouvet, A., Mermoz, S., Toan, T.L., Villard, L., Mathieu, R., Naidoo, L., Asner, G.P., 2018. An above-ground biomass map of African savannahs and woodlands at 25 m resolution derived from ALOS PALSAR. Remote Sens. Environ. 206, 156–173.

Brandt, M., Wigneron, J.P., Chave, J., Tagesson, T., Penuelas, J., Ciais, P., et al., 2018. Satellite passive microwaves reveal recent climate-induced carbon losses in African drylands. Nat. Ecol. Evol. 1.

Breiman, L., 1996. Bagging predictors. Mach. Learn. 24 (2), 123–140.

Breiman, L., 2001. Random forests. Mach. Learn. 45 (1), 5–32.

Carvalhais, N., Forkel, M., Khomik, M., Bellarby, J., Jung, M., Migliavacca, M., et al., 2014. Global covariation of carbon turnover times with climate in terrestrial ecosystems. Nature 514 (7521), 213.

Chave, J., Andalo, C., Brown, S., Cairns, M.A., Chambers, J.Q., Eamus, D., et al., 2005. Tree allometry and improved estimation of carbon stocks and balance in tropical forests. Oecologia 145 (1), 87–99.

Chave, J., Réjou-Méchain, M., Búrquez, A., Chidumayo, E., Colgan, M.S., Delitti, W.B., et al., 2014. Improved allometric models to estimate the aboveground biomass of tropical trees. Glob. Chang. Biol. 20 (10), 3177–3190.

Cui, Q., Shi, J., Du, J., Zhao, T., Xiong, C., 2015. An approach for monitoring global vegetation based on multiangular observations from SMOS. Ieee J. Sel. Top. Appl. Earth Obs. Remote. Sens. 8 (2), 604–616.

Englhart, S., Keuck, V., Siegert, F., 2011. Aboveground biomass retrieval in tropical forests—the potential of combined X-and L-band SAR data use. Remote Sens. Environ. 115 (5), 1260–1271.

FAO, 2000. FRA 2000: On Definitions of Forest and Forest Change, vol. 33 Forest Resource Assessment Programe Working Paper#33.

Frolking, S., Palace, M.W., Clark, D.B., Chambers, J.Q., Shugart, H.H., Hurtt, G.C., 2009. Forest disturbance and recovery: a general review in the context of spaceborne remote sensing of impacts on aboveground biomass and canopy structure. J. Geophys. Res. 114, G00E02.

Good, S.P., Caylor, K.K., 2011. Climatogical determinants of woody cover in Africa. Proc. Natl. Acad. Sci. U. S. A. 108, 4902–4907.

Hansen, M.C., Potapov, P.V., Moore, R., Hancher, M., Turubanova, S., Tyukavina, A., et al., 2013. High-resolution global maps of 21st-century forest cover change. Science 342 (6160), 850–853.

Harris, I.P.D.J., Jones, P.D., Osborn, T.J., Lister, D.H., 2014. Updated high-resolution grids of monthly climatic observations–the CRU TS3. 10 Dataset. Int. J. Climatol. 34 (3), 623–642.

Herrmann, S.M., Mohr, K.I., 2011. A continental-scale classification of rainfall seasonality regimes in Africa based on gridded precipitation and land surface temperature products. J. Appl. Meteorol. Climatol. 50 (12), 2504–2513.

Hu, T., Su, Y., Xue, B., Liu, J., Zhao, X., Fang, J., Guo, Q., 2016. Mapping global forest aboveground biomass with spaceborne LiDAR, optical imagery, and forest inventory data. Remote Sens. (Basel) 8 (7), 565.

Imhoff, M.L., 1995. Radar backscatter and biomass saturation: ramifications for global biomass inventory. IEEE Trans. Geosci. Remote Sens. 33, 511–518.

Johnson, M.O., Galbraith, D., Gloor, M., De Deurwaerder, H., Guimberteau, M., Rammig, A., Phillips, O.L., 2016. Variation in stem mortality rates determines patterns of above-ground biomass in Amazonian forests: Implications for dynamic global vegetation models. Glob. Chang. Biol. 22 (12), 3996–4013.

Kerr, Y.H., Waldteufel, P., Wigneron, J.-P., Delwart, S., Cabot, F., Boutin, J., et al., 2010. The SMOS mission: new tool for monitoring key elements of the global water cycle. Proc. IEEE 98, 666–687.

Kerr, Y.H., Waldteufel, P., Richaume, P., Wigneron, J.P., Ferrazzoli, P., Mahmoodi, A., Al Bitar, A., Cabot, F., Gruhier, C., Juglea, S.E., Leroux, D., Mialon, A., Delwart, S., 2012. The SMOS soil moisture retrieval algorithm. IEEE Trans. Geosci. Remote Sens. 50, 1367–1383 2012.

Konings, A.G., Piles, M., Rötzer, K., McColl, K.A., Chan, S.K., Entekhabi, D., 2016. Vegetation optical depth and scattering albedo retrieval using time series of dual-polarized L-band radiometer observations. Remote Sens. Environ. 172, 178–189.

Konings, A.G., Piles, M., Das, N., Entekhabi, D., 2017. L-band vegetation optical depth and effective scattering albedo estimation from SMAP. Remote Sens. Environ. 198, 460–470.

Lasky, J.R., Uriarte, M., Boukili, V.K., Erickson, D.L., John Kress, W., Chazdon, R.L., 2014. The relationship between tree biodiversity and biomass dynamics changes with tropical forest succession. Ecol. Lett. 17 (9), 1158–1167.

Liu, Y.Y., de Jeu, R.A., McCabe, M.F., Evans, J.P., van Dijk, A.I., 2011. Global long-term passive microwave satellite-based retrievals of vegetation optical depth. Geophys. Res. Lett. 38 (18).

Liu, Y.Y., Van Dijk, A.I., De Jeu, R.A., Canadell, J.G., McCabe, M.F., Evans, J.P., Wang, G., 2015. Recent reversal in loss of global terrestrial biomass. Nat. Clim. Chang. 5 (5), 470.

Mitchard, E.T., Saatchi, S.S., Baccini, A., Asner, G.P., Goetz, S.J., Harris, N.L., Brown, S., 2013. Uncertainty in the spatial distribution of tropical forest biomass: a comparison of pan-tropical maps. Carbon Balance Manage. 8 (1), 10.

Mori, A.S., Lertzman, K.P., Gustafsson, L., 2017. Biodiversity and ecosystem services in forest ecosystems: a research agenda for applied forest ecology. J. Appl. Ecol. 54 (1), 12–27.

Moron, V., Bigot, S., Roucou, P., 1995. Rainfall variability in subequatorial America and Africa and relationships with the main sea-surface temperature modes (1951–1990). Int. J. Climatol. 15 (12), 1297–1322.

Munzimi, Y.A., Hansen, M.C., Adusei, B., Senay, G.B., 2015. Characterizing Congo basin rainfall and climate using tropical rainfall measuring mission (trmm) satellite data and limited rain gauge ground observations. J. Appl. Meteorol. Climatol. 54 (3), 541–555.

Nicholson, S.E., 2000. The nature of rainfall variability over Africa on time scales of decades to millenia. Glob. Planet. Change 26 (1-3), 137–158.

Ninan, K.N., Inoue, M., 2013. Valuing forest ecosystem services: what we know and what we don't. Ecol. Econ. 93, 137–149.

Oliva, R., Daganzo, E., Richaume, P., Kerr, Y., Cabot, F., Soldo, Y., et al., 2016. Status of radio frequency interference (RFI) in the 1400–1427 MHz passive band based on six years of SMOS mission. Remote Sens. Environ. 180, 64–75.

Olson, D.M., Dinerstein, E., Wikramanayake, E.D., Burgess, N.D., Powell, G.V., Underwood, E.C., et al., 2001. Terrestrial Ecoregions of the World: a New Map of Life on Earth: a new global map of terrestrial ecoregions provides an innovative tool for conserving biodiversity. BioScience 51 (11), 933–938.

Poorter, L., Sande, M.V.D., Thompson, J., Arets, E.J.M.M., Alarcón, A., Álvarez-Sánchez, J., et al., 2015. Diversity enhances carbon storage in tropical forests. Glob. Ecol. Biogeogr. 24 (11), 1314–1328.

Rahmoune, R., Ferrazzoli, P., Singh, Y.K., Kerr, Y.H., Richaume, P., Al Bitar, A., 2014. SMOS retrieval results over forests: comparisons with independent measurements. Ieee J. Sel. Top. Appl. Earth Obs. Remote. Sens. 7 (9), 3858–3866.

Reboita, M.S., Gan, M.A., da Rocha, R.P., Ambrizzi, T., 2010. Regimes de precipitação na América do Sul: uma revisão bibliográfica. Rev. Bras. Meteorol. 25 (2).

Rodríguez-Fernández, N.J., Mialon, A., Mermoz, S., Bouvet, A., Richaume, P., Al Bitar, A., Al-Yaari, A., Brandt, M., Kaminski, T., Le Toan, T., Kerr, Y.H., Wigneron, J.-P., 2018. An evaluation of SMOS L-band vegetation optical depth (L-VOD) data sets: high sensitivity of L-VOD to above-ground biomass in Africa. Biogeosciences 15, 4627–4645. https://doi.org/10.5194/bg-15-4627-2018.

Saatchi, S., Malhi, Y., Zutta, B., Buermann, W., Anderson, L.O., Araujo, A.M., et al., 2009. Mapping landscape scale variations of forest structure, biomass, and productivity in Amazonia. Biogeosci. Discuss. 6 (3), 5461.

Saatchi, S.S., Harris, N.L., Brown, S., Lefsky, M., Mitchard, E.T., Salas, W., et al., 2011. Benchmark map of forest carbon stocks in tropical regions across three continents. Proc. Natl. Acad. Sci. 108 (24), 9899–9904.

Santoro, M., Beaudoin, A., Beer, C., Cartus, O., Fransson, J.E., Hall, R.J., et al., 2015.

Forest growing stock volume of the northern hemisphere: spatially explicit estimates for 2010 derived from Envisat ASAR. Remote Sens. Environ. 168, 316–334.
Santos, J.R., Freitas, C.C., Araujo, L.S., Dutra, L.V., Mura, J.C., Gama, F.F., et al., 2003. Airborne P-band SAR applied to the aboveground biomass studies in the Brazilian tropical rainforest. Remote Sens. Environ. 87, 482–493.
Simard, M., Pinto, N., Fisher, J.B., Baccini, A., 2011. Mapping forest canopy height globally with spaceborne lidar. J. Geophys. Res. Biogeosci. 116 (G4).
Stegen, J.C., Swenson, N.G., Enquist, B.J., White, E.P., Phillips, O.L., Jørgensen, P.M., et al., 2011. Variation in above-ground forest biomass across broad climatic gradients. Glob. Ecol. Biogeogr. 20 (5), 744–754.
Strassburg, B.B., Kelly, A., Balmford, A., Davies, R.G., Gibbs, H.K., Lovett, A., et al., 2010. Global congruence of carbon storage and biodiversity in terrestrial ecosystems. Conserv. Lett. 3 (2), 98–105.
Udvardy, M.D.F., 1975. A classification of the biogeographical provinces of the world. International Union of Conservation of Nature and Natural Resources. IUCN Occasional Paper no. 18, Morges (Switzerland).
Vittucci, C., Ferrazzoli, P., Kerr, Y., Richaume, P., Guerriero, L., Rahmoune, R., Vaglio Laurin, G., 2016. SMOS retrieval over forests: exploitation of optical depth and tests of soil moisture estimates. Remote Sens. Environ. 180, 115–127.
Vittucci, C., Ferrazzoli, P., Kerr, Y., Richaume, P., Vaglio Laurin, G., Guerriero, L., 2018. Analysis of vegetation optical depth and soil moisture retrieved by SMOS over tropical forests. IEEE Geosci. Remote Sens. Lett. https://doi.org/10.1109/LGRS.2018.2878359.
Wagner, F., Rossi, V., Stahl, C., Bonal, D., Herault, B., 2012. Water availability is the main climate driver of neotropical tree growth. PLoS One 7 (4) e34074.
Wang, H., Ouchi, K., Watanabe, M., Shimada, M., Tadono, T., Rosenqvist, A., Romshoo, S.A., Matsuoka, M., Moriyama, T., Uratsuka, S., 2006. In search of the statistical properties of high-resolution polarimetric SAR data for the measurements of forest biomass beyond the RCS saturation limits. IEEE Geosci. Remote Sens. Lett. 3 (4), 495–499.
Williams, C.A., Hanan, N., Scholes, R.J., Kutsch, W., 2009. Complexity in water and carbon dioxide fluxes following rain pulses in an African savanna. Oecologia 161, 469–480.